Polish Journal of Medical Physics and Engineering
The Journal of Polish Society of Medical Physics
ISSN 1898-0309, doi: 10.2478/pjmpe-2024-0029

December 2024
Vol 30, Issue 4

Scientific Paper

# Low-cost 3D vision-based triangulation system for ultrasonic probe positioning

Szymon CYGAN [1,ABCDEF,*], Mateusz URBAN[1,BDF], Anna CZYŻYK[1,BCF], Jakub ŻMIGRODZKI [1,AEF]

[1]*Warsaw University of Technology, Institute of Metrology and Biomedical Engineering, Warsaw, Poland*

[*]*Corresponding author: Szymon Cygan; szymon.cygan@pw.edu.pl*

(received 19 August 2024; revised 1 December 2024; accepted 3 December 2024)

## Abstract

*Introduction:* In ultrasonic imaging, such as echocardiography, accurately positioning the probe in relation to the patient's body or an external coordinate system is typically done manually. However, when developing speckle-tracking methods for echocardiology, ensuring consistency in probe positioning is essential for reliable data interpretation. To address this challenge, we present a vision-based system and method for probe positioning in this study.

*Materials and Methods:* Our system comprises two cameras, a calibration frame with eight markers of known coordinates in the frames' local coordinate system, and a probe holder with four markers. The calibration process involves image segmentation via region growing and extraction of the camera projection matrices. Subsequently, our positioning method also utilises marker segmentation, followed by estimating the markers' positions using triangulation.

*Results:* To evaluate the system's performance, we conducted tests using a validation plate with five coplanar circular markers. The distances between each pair of points were calculated, and their errors compared to the true distances were found to be within a maximum of 0.7 mm. This level of accuracy is comparable to ultrasonic imaging resolution and thus deemed sufficient for the intended purpose.

*Conclusion:* For those interested in replicating or modifying our methods, the supplementary material includes the complete design of the calibration frame and the Matlab code.

**Keywords**: triangulation; image analysis; direct linear transform; phantom for echocardiography.

## Introduction

Ultrasonic imaging (US), including echocardiography, relies on manual control of the probe's position by a physician or medical technician/sonographer to capture the desired section view of the examined organ. This process demands a deep understanding of anatomy and expertise in operating the ultrasound scanning probe. Unlike tomographic techniques such as computed tomography and magnetic resonance imaging, ultrasonic imaging is heavily reliant on observer input.[1-3]

Various research studies have explored methods for quantifying ultrasound (US) probe positioning.[3-5] These methods can be categorised based on the tracking approach used, including optical, electromagnetic, acoustic, mechanical, and inertial systems.[5] Optical tracking, which monitors an object in all six degrees of freedom (DOF), is considered the most precise.[5] It relies on visible or infrared light, either reflected or emitted by markers and thus requires an unobstructed line-of-sight between the cameras and the markers. Electromagnetic tracking systems also provide 6-DOF information and are not constrained by the line-of-sight requirement. Acoustic tracking systems estimate 3D positions by measuring the time-of-flight of ultrasound pulses transmitted by a probe and received by at least three sensors. Mechanical tracking systems, often utilising robotic arms, combine active positioning with position monitoring, offering a unique approach compared to other systems. Inertial tracking systems, which employ single-chip inertial measurement units (IMUs), provide data on changes in position (such as accelerations and angular velocities) rather than absolute 3D coordinates.

Motion tracking solutions have been widely applied in various ultrasound imaging applications, including freehand 3D ultrasound imaging, ultrasound image fusion, and ultrasound-guided interventions and treatments. However, the integration of methods for generating 3D ultrasound images using tracked 2D probes in real-world space has been limited by advances in the development of dedicated 3D ultrasound probes.[6,7]

Beyond potential routine medical applications, several research fields stand to benefit from ultrasound probe tracking capabilities. Left ventricular phantoms, for instance, are



Authors' contribution: A – Research concept and design, B – Collection and/or assembly of data, C – Data analysis and interpretation, D – Writing the article, E – Critical revision of the article, F – Final approval of the article.

invaluable in refining speckle-tracking echocardiography methods.[8-9] However, precise probe positioning is essential to ensure data consistency and repeatability in such studies. Unfortunately, this critical aspect has often been neglected in published research.[10-13]

To address this issue, we propose a solution for accurately positioning the ultrasonic probe and imaging plane within a laboratory setup for left ventricular phantom imaging. Our approach involves employing two cameras strategically positioned to cover the entire measurement volume, along with a rigid markers-frame for calibrating the camera setup. We utilise the Direct Linear Transformation method to calibrate the cameras based on the known marker locations on the frame. Subsequently, we employ the triangulation method to determine the unknown positions of markers placed on the ultrasonic probe holder.

## Materials and Methods

### Positioning system

The ultrasonic probe positioning system, shown in **Figure 1**, was designed for an existing left ventricular phantom system for speckle-tracking echocardiography research.[10,13,14] This purpose defined the required measurement volume to be covered as having dimensions of approximately 300 × 250 × 150 mm (depth × width × height). To cover this volume, two general-purpose web cameras (Live! Cam Sync, Creative, Singapore) were used with 1920 × 1080 pixel resolution. The use of simple, low-cost cameras in this work stems from the original concept of evaluating their performance as a viable alternative to professional systems.

The cameras were placed approximately 370 mm above the tank and 370 mm horizontally from the centre of the tank, spaced approximately 600 mm from each other. Their positioning does not have to be precise, only so that their field of view covers the whole of the measurement volume.

### Setup calibration method

For the purpose of camera calibration, a frame, shown in **Figure 2**, with eight markers with known coordinates, was created. The frame was designed using Autodesk Inventor 2024 software. To ensure precise positioning, the frame was designed as four plates produced by laser cutting of a 4 mm thick medium-density fibre board (MDF). The real-world coordinates of the markers are given in **Table 1**. The internal intersection point of the back, bottom and left plate was chosen as the centre of the real-world coordinate system; the X axis was defined by the joining line of the bottom and the side plate, and the XY plane was defined by the bottom plate. The positions of all the markers are defined by the design of the plates. The 2D outlines of the plates are provided in svg files, ready to be used for laser cutting[†]. The precise positioning of the frame on the phantom tank is achieved by three protrusions reaching down, below the bottom of the frame, that ensure proper alignment of the frame with the rear and side wall of the tank. The markers were designed as spheres with 20 mm diameter chamfered by 2 mm with a 5 mm hole allowing for their fixing to the calibration frame using standard M5 bolts. Marker geometries are provided as a stl file in the supplementary material.

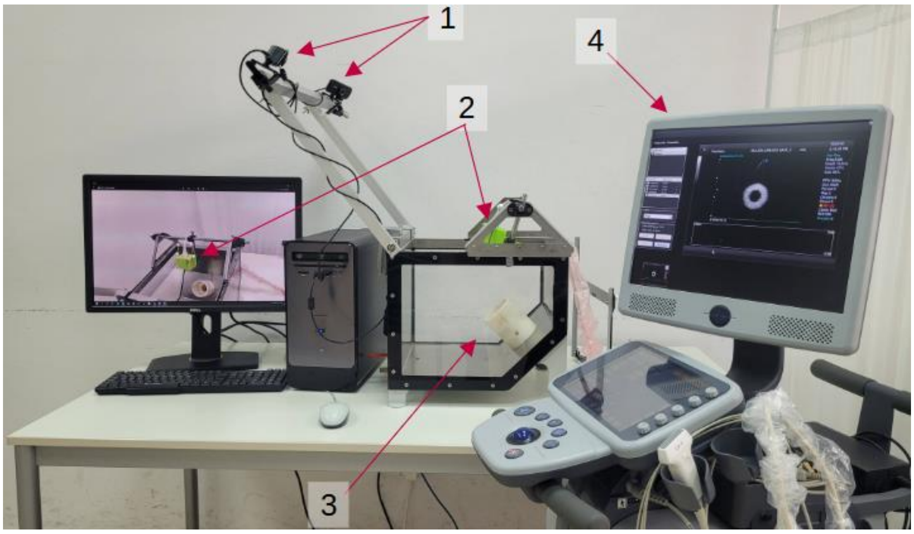


**Figure 1. The setup designed for positioning of the ultrasonic probe. 1 – two cameras fixed on a positioning frame, 2 – ultrasonic probe holder on the phantom tank (on the PC screen as registered by one of the cameras), 3 – phantom fixing socket in the phantom tank (here shown empty), 4 – ultrasound scanner displaying an earlier registered phantom short axis view.**

[†] The supplementary material with designs, code and example images is provided at: https://drive.google.com/file/d/1gqvBGmIdrNiWcGsKTJxo_MHrXJ0jYnT4/view?usp=sharing


**Figure 2. Calibration frame with eight visible markers. Their numbering defines the order of assigning coordinates. The assumed real-world coordinate system is marked by the axes on the CAD design visualisation (left). The real frame with markers shown on the phantom tank (right).**

The proposed method for setup calibration has been implemented in the Matlab 2022b environment (Mathworks, USA). Schematics of the method are shown in **Figure 3**.

The calibration process begins with capturing static images from both cameras, either through a standard camera application or using a MATLAB function for image acquisition. At this stage, it is essential to verify the quality of the captured images. All markers must be clearly visible, and the lighting conditions should ensure a clear distinction between the markers and their background. While a more quantitative evaluation of image quality will be performed during the parameter tuning stage, conducting a qualitative assessment at this point can significantly streamline the overall process.

The next step requires the user to point the markers in the designated order (see **Figure 2**) on both images in order to match each marker with the provided real-world coordinates. For this purpose, the Matlab' getpts' function, which is available in the 'Image Processing and Computer Vision' Toolbox, is used.

As the process of pointing markers is done by hand and thus its precision is variable, a segmentation step has been included in the process. The image-plane coordinates provided manually by the user are used as starting points (seeds) for the segmentation by region growing, carried out using the 'regiongrowing' function available at [15]. The results of segmentation depend on the image contrast and selected intensity distance threshold (maximum difference of intensity between the seed point and the pixels joining the segmented region).

The segmentation method returns binary masks with 'true' pixels where the marker has been identified. Centroids of those masks are obtained using the 'regionprops' Matlab function. Those centroids are subsequently used as image-plane coordinates of the markers for further processing. This is based on the assumption that spherical markers observed from any direction are seen as circular, with centroids being projections of the 3D location of the centre of mass.

**Table 1. Real-world coordinates of the markers shown in Figure 2.**

| Marker no. | 1 | 2 | 3 | 4 | 5 | 6 | 7 | 8 |
|---|---|---|---|---|---|---|---|---|
| X [mm] | 246.1 | 246.1 | 51.1 | 71.1 | 51.1 | 8 | 8 | 8 |
| Y [mm] | 16.1 | 311.1 | 281.1 | 166.1 | 51.1 | 21.1 | 166.1 | 311.1 |
| Z [mm] | 8 | 8 | 8 | 8 | 8 | 235 | 235 | 235 |

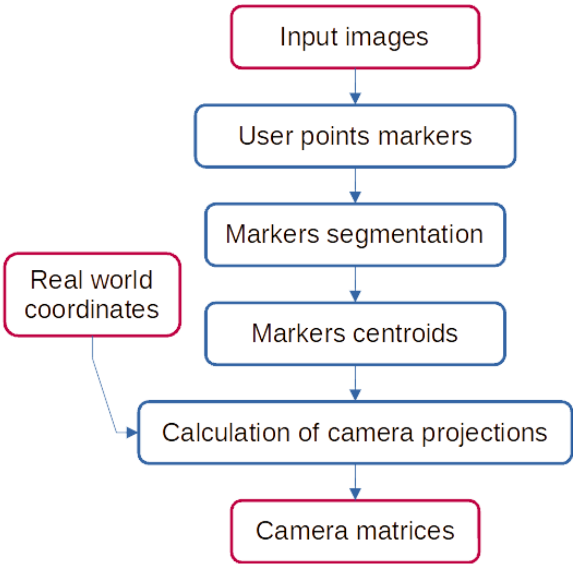


**Figure 3. Schematics of the system calibration method.**

The crucial step in setup calibration is the calculation of camera projection matrices using a Direct Linear Transformation.[16,17] This method makes use of known real-world coordinates of objects visible on an image (markers' coordinates given in **Table 1**) and their positions on the image, obtained in the previous step, to reconstruct the parameters of the camera position and image deformation. This step is carried out using the 'estimateCameraProjection' Matlab function available in the 'Image Processing and Computer Vision' Toolbox (or the 'estimateCameraMatrix' function up to Matlab version 2022a). Returned projection matrices are the output of the calibration process, which is then saved in a separate file to be used as necessary input during the probe positioning process carried out with the same setting of cameras. The camera projection estimation function also returns the reprojection error values for each analysed point, which is the difference between the location of the point identified in the image and the point projected onto the image plane.

## Image processing parameter tuning

As mentioned above, the threshold value used in region-growing segmentation and the size of the structuring element in the morphological closing operation influence the process of localising the centroid of the markers. For this reason, a separate Matlab script has been provided that establishes preferred settings based on the minimum mean reprojection error obtained during the system calibration process. It is performed for a user-defined range of disk radii and region-growing threshold values. The script iterates through each combination of these parameters to evaluate their impact on the mean reprojection error.

Within the nested loops, region-growing segmentation is performed on both images, followed by the closing operation, and centroids of segmented regions are computed. Camera projection matrices are estimated using the localised centroids and provided real world coordinates of the markers on the frame, and reprojection errors are computed.

Finally, the mean reprojection error values for different parameter combinations are used to evaluate the influence of each parameter on the calibration process. The error values are plotted as a surface plot, with the structuring disk size and region growing limit on the x and y axes, respectively, and the mean reprojection error value on the z-axis.

## Probe positioning method

For the positioning of the probe, a dedicated 3D printed holder was designed using the exact shape of the probe used in the setup - SA4-2/24 (Ultrasonix, Richmond, Canada). The probe holder was produced using black acrylonitrile-butadiene-styrene filament (ABS). It was equipped with four protrusions supporting four 10 mm markers 3D printed using white polylactide filament (PLA). The markers were attached in the same plane as the imaging plane (**Figure 4**). Four markers were used, so except for reprojection errors, the coplanarity test can also provide information on possible positioning errors.

In the provided script, the process of probe positioning starts with acquisitions of two stationary images of the holder taken with the two cameras with available projections matrices obtained during calibration. This acquisition process can be carried out similarly to the calibration phase, using either a standard image capture software or from within the Matlab environment. As the presented application is designed to register a stationary scene, the synchronisation of image capture is not necessary.

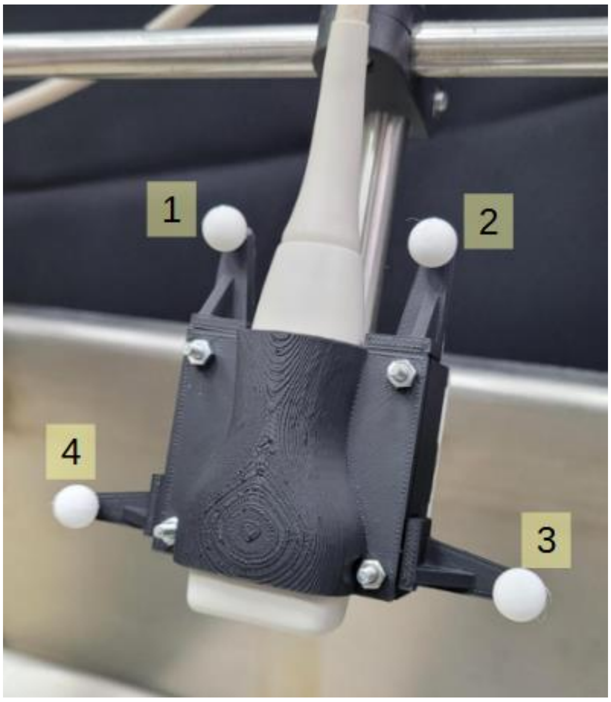


**Figure 4. The probe holder with four markers used for probe positioning.**

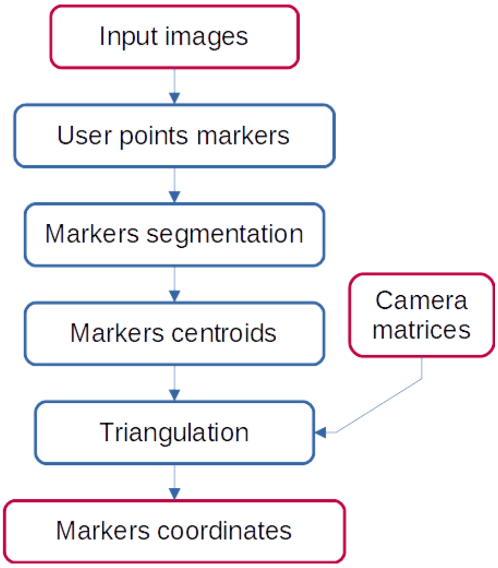


**Figure 5. Schematics of the probe positioning method (right).**

The initial processing of the images, as shown in **Figure 5**, follows the same pattern as during calibration, leading to the obtaining of markers' positions on the images (image coordinates). This process includes pointing the markers by the user, segmenting them using the region growing method, applying morphological closing operations, and obtaining centroids of the binary masks of the markers.

Estimation of real-world coordinates of the markers registered in the input images is carried out using a triangulation method[18] that uses the camera projection matrices obtained during calibration and markers coordinates in the image plane to reconstruct markers' positions. This step is carried out using the 'triangulate' Matlab function available in the 'Image Processing and Computer Vision' Toolbox. The triangulation function also returns the reprojection error values for each analysed point, which is the difference between the location of the input point (marker centre from segmentation) in the image and the point location estimated by triangulation, projected onto the image plane.

The real world coordinates of the markers' centres are used to calculate the equation of the imaging plane and to verify the coplanarity of the obtained centre points.

A plane is fitted to the points using singular value decomposition (SVD). The three matrices returned by the SVD decomposition are used to extract the normal vector [a, b, c] of the plane from the right singular vectors. This provides the equation of the plane in the form $ax + by + cz + d = 0$, where d is the negative distance from the origin.

The coplanarity error for each point is calculated using the plane equation. For each identified marker centre point described by the coordinate values (x, y, z), the coplanarity error is given by $|ax + by + cz + d|$.

## Validation of the proposed method

To validate and assess the precision of the proposed method, a flat validation plate was used with 5 circular markers, 10 mm in diameter spaced, as shown in **Figure 6**. The precision of plate dimensions measurement was ± 0.1 mm. The positioning procedure was applied to images of the plate placed in three different positions in the laboratory setup. Euclidean distances between various pairs of markers were then calculated, and results were verified against the known real-world distances. A test to verify if the resulting points are coplanar was also performed, and the tolerance required to confirm their coplanarity was identified.

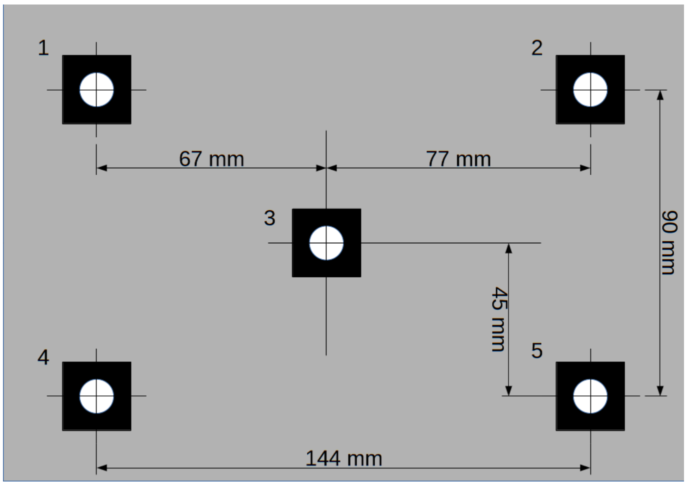


**Figure 6. The validation plate with 10 mm diameter markers.**

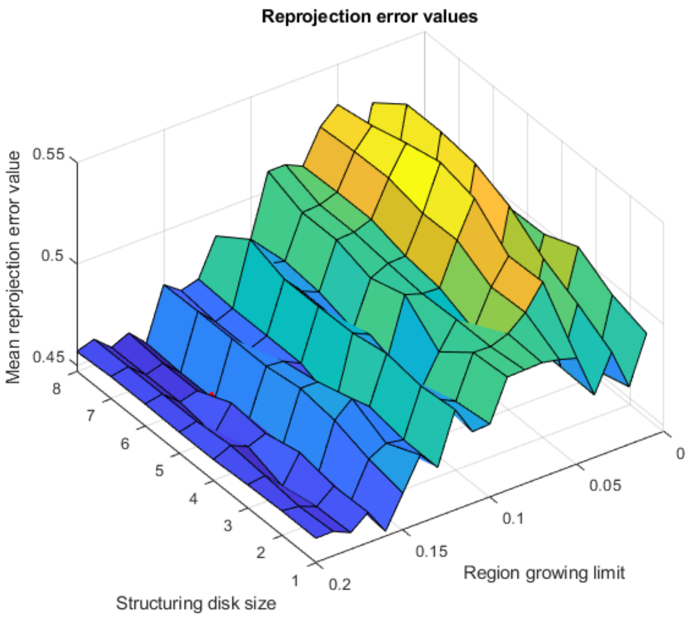


**Figure 7. Surface plot of mean reprojection errors in the calibration process as a function of structuring disc size and the relative threshold used in the segmentation process using the region growing method.**

# Results

## Parameter tuning

The parameter tuning for calibration and positioning procedures was carried out for values of the region growing relative threshold, defining the maximum intensity difference between the seed pixel and the pixels attached to the mask, ranging from 0.01 to 0.2 with 0.01 step (20 values) and for closing structuring disc element with radii ranging from 1 to 8 pixels (8 integer values). The obtained surface plot of the mean reprojection error values as a function of the two parameters is shown in **Figure 7**.

The obtained Mean Reprojection Error range was from 0.4469 to 0.5419, with the minimum obtained for structuring disk size 6 and region growing relative threshold: 0.16.

## Setup calibration

System calibration was carried out as described in the **Materials and Methods** section using region growing threshold value selected based on the Parameter tuning process thr = 0.16, and the structuring disc radius of 6. The results of the markers' segmentation were visualised for inspection, as shown in **Figure 8**, and zoomed in on **Figure 9**.

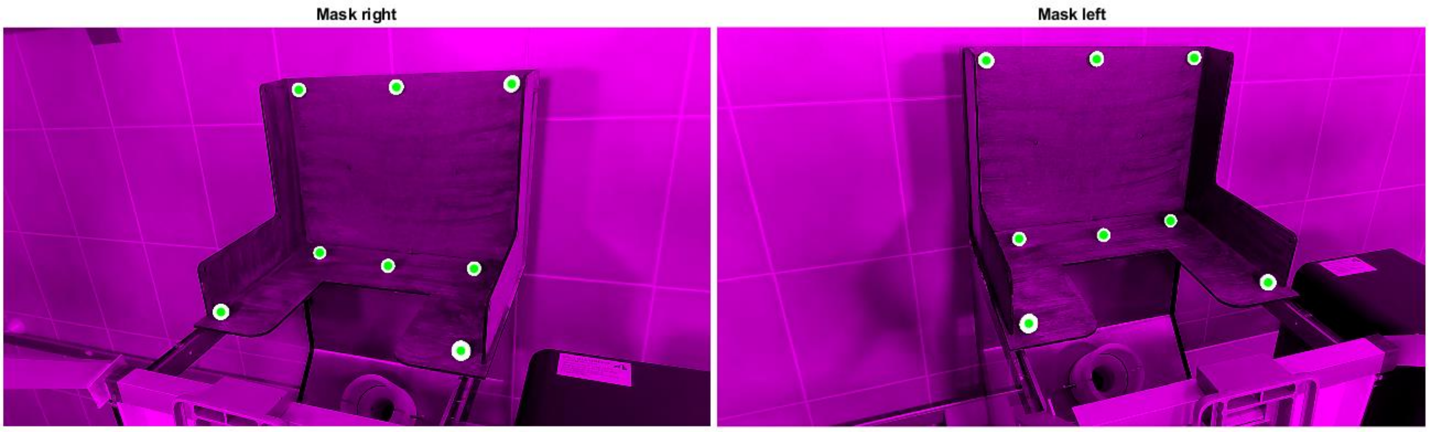


**Figure 8. Acquired images of the calibration frame on the phantom tank with overlayed masks of identified markers.**

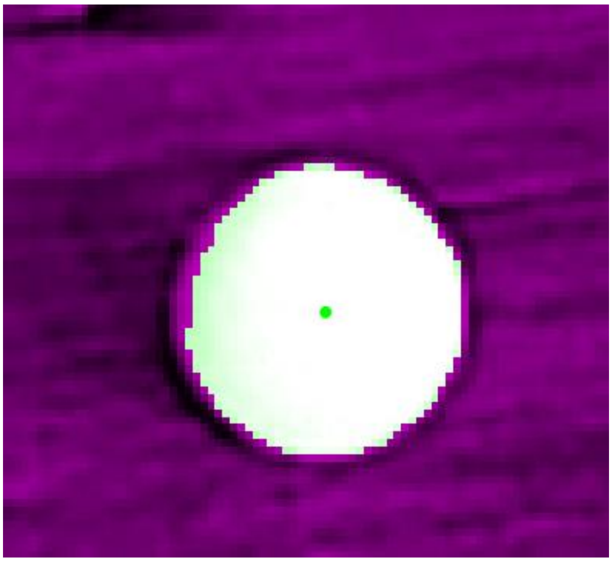

**Figure 9. Zoomed in marker no. 3 as seen from the 'left' camera (Figure 8).**

Camera projection matrices were estimated and reprojection errors were calculated. Obtained values were saved as input for the positioning method. Error values for each marker and both views (left and right) are given in **Table 2**.

**Table 2. Reprojection errors, in [mm], returned by the function estimating camera projection matrices.**

| Marker no. | 1 | 2 | 3 | 4 | 5 | 6 | 7 | 8 |
|---|---|---|---|---|---|---|---|---|
| Repr. error Left view | 0.289 | 0.305 | 0.704 | 0.301 | 0.439 | 0.278 | 0.592 | 0.459 |
| Repr. error Right view | 0.420 | 0.370 | 0.603 | 0.542 | 0.581 | 0.184 | 0.527 | 0.362 |

## Validation

The validation process was carried out using the validation plate shown in **Figure 6**. Distance estimation errors between all five markers for three different placements of the plate are presented in **Table 3**. The position tolerances required to assume the coplanarity of the five markers are given in **Table 4**.

**Table 3. Errors of positioning results [mm], calculated as the differences between the real-world distances between markers visible on the validation plate and the distances returned by the proposed positioning method. Errors were obtained for three separate cases of validation plate positioning.**

| | Marker no. | 1 | 2 | 3 | 4 | 5 |
|---|---|---|---|---|---|---|
| Case 1 | 1 | 0 | 0.415 | 1.104 | -0.185 | 0.996 |
| | 2 | 0.415 | 0 | -0.136 | 0.448 | 1.152 |
| | 3 | 1.104 | -0.136 | 0 | 0.531 | -0.125 |
| | 4 | -0.186 | 0.448 | 0.531 | 0 | 0.692 |
| | 5 | 0.997 | 1.152 | -0.125 | 0.692 | 0 |
| Case 2 | 1 | 0 | -0.262 | 0.401 | -0.120 | 1.933 |
| | 2 | -0.262 | 0 | -0.738 | -1.096 | 0.473 |
| | 3 | 0.401 | -0.738 | 0 | -0.356 | 1.558 |
| | 4 | -0.120 | -1.096 | -0.356 | 0 | 1.06 |
| | 5 | 1.933 | 0.473 | 1.558 | 1.06 | 0 |
| Case 3 | 1 | 0 | 1.293 | 0.85 | 0.494 | 2.124 |
| | 2 | 1.293 | 0 | 0.832 | 1.075 | 1.039 |
| | 3 | 0.85 | 0.832 | 0 | 0.25 | 1.287 |
| | 4 | 0.494 | 1.075 | 0.25 | 0 | 1.53 |
| | 5 | 2.124 | 1.04 | 1.287 | 1.53 | 0 |

**Table 4. Tolerances required to assume coplanarity of each of the validation markers for each of the 3 cases.**

| Marker no. \ Case no. | 1 | 2 | 3 |
|---|---|---|---|
| 1 | 0.352 | 0.729 | 0.17 |
| 2 | 0.26 | 0.274 | 0.507 |
| 3 | 0.177 | 0.902 | 0.68 |
| 4 | 0.258 | 0.242 | 0.534 |
| 5 | 0.343 | 0.688 | 0.19 |

## Probe positioning

Sample probe positioning results are presented as an example of the capabilities of the proposed method. The probe was set randomly over the tank, as it would be placed when imaging a left ventricular phantom. The obtained coordinates of the markers and their respective reprojection errors are given in **Table 5**.

**Table 5. Obtained coordinates of the four markers used to position the probe, as visible in Figure 4.**

| Marker no. | 1 | 2 | 3 | 4 |
|---|---|---|---|---|
| X [mm] | 150.6 | 213.6 | 53.6 | 150.6 |
| Y [mm] | 150.5 | 261.2 | 54.5 | 150.5 |
| Z [mm] | 173.6 | 188.1 | -10.5 | 173.6 |
| Reprojection errors [mm] | 0.6 | 1.15 | 0.3 | 0.51 |
| Coplanarity errors [mm] | 0.65 | 0.65 | 0.3 | 0.3 |

## Discussion

Results of the segmentation of markers in the calibration frame images suggest that the quality of segmentation is crucial to obtaining precise calibration of the system. Reprojection errors reported in **Table 2** do reach 0.7 mm and are of similar magnitude as possible errors of localising the centres of markers via centroids of masks obtained from segmentation.

The parameter tuning process showed that the reprojection errors are sensitive to the region growing segmentation threshold used and much less to the structuring disc radius used to perform closing operation before localising centroids of the marker views. This tuning process should be performed for each imaging conditions as the appropriate threshold value depends on the lighting conditions during image acquisition.

Reprojection errors obtained during calibration are of similar magnitude as the distance estimation errors obtained in the validation process as well as the coplanarity tolerance required to assume the validation markers are considered as coplanar. Estimation of distances between markers returns similar results regardless of the position of the validation plate, which suggests that the position estimates remain consistent throughout the entire field of view.

The calibration process resulted in a reported reprojection error of 1.15 mm during probe positioning. This level of precision can be considered adequate for 2D ultrasonic imaging, where the elevational "thickness" of the imaging plane spans several millimeters.[19] Such repeatability ensures that the same area of the phantom can be examined consistently, even after resetting the experimental setup. Notably, the 1.15 mm reprojection error is comparable to the precision achieved by a professional, commercially available marker-based motion capture system described in [20]. While that system operates on similar principles, it is designed for significantly larger working volumes, which inherently results in higher relative precision. The ultrasonic probe positioning system described in [21] achieves significantly higher precision (at the level of 0.2 mm), but this is achieved by using a dedicated Atracsys easyTrack 500 tracking system. Given the simplicity and cost-effectiveness of the solution proposed in this work, the achieved residual error is both acceptable and satisfactory for imaging left ventricular phantoms. However, for other applications, a case-by-case analysis is necessary to determine whether the precision meets the specific requirements.

## Conclusions

The proposed system for ultrasonic probe positioning over a left ventricular phantom tank enables the quantification of probe orientation in the coordinate system of the tank and thus recreating the conditions of echocardiographic data acquisition after resetting the phantom setup or exchanging the phantom. This solution can be a useful addition to phantom-based research in the field of speckle tracking echocardiography, tissue Doppler imaging and others, where imaging data with as much reference as possible is required. This approach can also be useful in the field of machine learning applications to echocardiography, where large quantities of data are required for training the models.[22] The use of phantom data could serve as a pre-training method, significantly reducing the amount of patient data required to train the machine learning methods.

The 3D positioning method, combined with the provided calibration frame, offers adaptability for a wide range of applications. By acquiring synchronised video recordings from the two calibrated cameras, the motion of markers can be tracked, and motion capture can be performed using the supplied code for diverse purposes. With minor modifications, including software-controlled synchronised image capture, our team successfully tested the proposed method for registering patients' chest movements during breathing, highlighting its potential application in gated radiotherapy. The initial results have been encouraging, demonstrating the method's versatility and promise.

The project's next stage will involve incorporating a lens distortion correction procedure, followed by two distinct development paths. The first path aims to create a more universal and versatile solution by enabling support for a greater number of cameras. This will include reimplementing the code in an open-source Python environment, making it more accessible and widely available to the research community. The second path will focus on deeper integration with the experimental setup for echocardiography phantom data acquisition. This will enable the creation of a comprehensive database of echocardiographic images, serving as a critical resource for advancing machine learning-based strain imaging techniques.

## Funding

The work was supported by a research grant no. 504/04540/1142/43.050001 of the Scientific Council of the Discipline of Biomedical Engineering of the Warsaw University of Technology

## Competing interests

The authors have no conflicts of interest, either financial or personal, regarding this work.

## Availability of data and materials

The supplementary material with designs, code and example images is provided at:
https://drive.google.com/file/d/1gqvBGmIdrNiWcGsKTJxo_MHrXJ0jYnT4/view?usp=sharing

## References

1. Chetboul V, Athanassiadis N, Concordet D, et al. Observer-dependent variability of quantitative clinical endpoints: the example of canine echocardiography. Vet Pharm & Therapeutics. 2004;27(1):49-56. https://doi.org//10.1046/j.0140-7783.2003.00543.x
2. Kunz P, Kiesl S, Groß S, Kauczor HU, Schmidmaier G, Fischer C. Intra-observer and Device-Dependent Inter-observer Reliability of Contrast-Enhanced Ultrasound for Muscle Perfusion Quantification. Ultrasound in Medicine & Biology. 2020;46(2):275-285. https://doi.org//10.1016/j.ultrasmedbio.2019.10.007
3. Serago CF, Chungbin SJ, Buskirk SJ, Ezzell GA, Collie AC, Vora SA. Initial experience with ultrasound localisation for positioning prostate cancer patients for external beam radiotherapy. International Journal of Radiation Oncology*Biology*Physics. 2002;53(5):1130-1138. https://doi.org//10.1016/s0360-3016(02)02826-2
4. Toporek G, Wang H, Balicki M, Xie H. Autonomous image-based ultrasound probe positioning via deep learning. EasyChair Preprints. Published online May 8, 2018. https://doi.org//10.29007/dj33
5. Peng C, Cai Q, Chen M, Jiang X. Recent Advances in Tracking Devices for Biomedical Ultrasound Imaging Applications. Micromachines. 2022;13(11):1855. https://doi.org//10.3390/mi13111855
6. Ali A, Logeswaran R. A visual probe localisation and calibration system for cost-effective computer-aided 3D ultrasound. Computers in Biology and Medicine. 2007;37(8):1141-1147. https://doi.org//10.1016/j.compbiomed.2006.10.003
7. De Lorenzo D, Vaccarella A, Khreis G, Moennich H, Ferrigno G, De Momi E. Accurate calibration method for 3D freehand ultrasound probe using virtual plane. Medical Physics. 2011;38(12):6710-6720. https://doi.org//10.1118/1.3663674
8. Rocchi M, Ingram M, Claus P, D'hooge J, Meyns B, Fresiello L. Use of 3D anatomical models in mock circulatory loops for cardiac medical device testing. Artificial Organs. 2022;47(2):260-272. https://doi.org//10.1111/aor.14433
9. Okrasinski SJ, Ramachandran B, Konofagou EE. Assessment of myocardial elastography performance in phantoms under combined physiologic motion configurations with preliminaryin vivofeasibility. Phys Med Biol. 2012;57(17):5633-5650. https://doi.org//10.1088/0031-9155/57/17/5633
10. Heyde B, Cygan S, Hon Fai Choi, et al. Regional cardiac motion and strain estimation in three-dimensional echocardiography: a validation study in thick-walled univentricular phantoms. IEEE Trans Ultrason, Ferroelect, Freq Contr. 2012;59(4):668-682. https://doi.org//10.1109/tuffc.2012.2245
11. Hjertaas JJ, Fosså H, Dybdahl GL, Grüner R, Lunde P, Matre K. Accuracy of Real-Time Single- and Multi-Beat 3-D Speckle Tracking Echocardiography In Vitro. Ultrasound in Medicine &vBiology. 2013;39(6):1006-1014. https://doi.org//10.1016/j.ultrasmedbio.2013.01.010
12. Lesniak-Plewinska B, Cygan S, Kaluzynski K, et al. A Dual-Chamber, Thick-Walled Cardiac Phantom for Use in Cardiac Motion and Deformation Imaging by Ultrasound. Ultrasound in Medicine & Biology. 2010;36(7):1145-1156. https://doi.org//10.1016/j.ultrasmedbio.2010.04.008
13. Cygan S, Werys K, Błaszczyk Ł, Kubik T, Kałużyński K. Left ventricle phantom and experimental setup for MRI and echocardiography – Preliminary results of data acquisitions. Biocybernetics and Biomedical Engineering. 2014;34(1):19-24. https://doi.org//10.1016/j.bbe.2013.12.002
14. Cygan S, Kumor M, Żmigrodzki J, Leśniak-Plewińska B, Kowalski M, Kałużyński K. Left ventricular phantoms with inclusions simulating transmural and non-transmural infarctions: FEM and EchoPAC study. Duric N, Heyde B, eds. SPIE Proceedings. 2017;10139:1013918. https://doi.org//10.1117/12.2254350

15. Kroon DJ. Region Growing (https://www.mathworks.com/matlabcentral/fileexchange/19084-region-growing). MATLAB Central File Exchange. Retrieved January 11, 2023.

16. Kolahi A, Hoviattalab M, Rezaeian T, Alizadeh M, Bostan M, Mokhtarzadeh H. Design of a marker-based human motion tracking system. Biomedical Signal Processing and Control. 2007;2(1):59-67. https://doi.org//10.1016/j.bspc.2007.02.001

17. Abdel-Aziz YI, Karara HM. Direct Linear Transformation from Comparator Coordinates into Object Space Coordinates in Close-Range Photogrammetry. photogramm eng remote sensing. 2015;81(2):103-107. https://doi.org//10.14358/pers.81.2.103

18. Rahimian P, Kearney JK. Optimal Camera Placement for Motion Capture Systems. IEEE Trans Visual Comput Graphics. 2017;23(3):1209-1221. https://doi.org//10.1109/tvcg.2016.2637334

19. Żmigrodzki J, Cygan S, Leśniak-Plewińska B, Kowalski M, Kałużyński K. Effect of Transmural Extent of the Simulated Infarction in a Left Ventricular Model on Displacement and Strain Distribution Estimated from Synthetic Ultrasonic Data. Ultrasound in Medicine & Biology. 2017;43(1):206-217. https://doi.org//10.1016/j.ultrasmedbio.2016.08.017

20. Das K, de Paula Oliveira T, Newell J. Comparison of markerless and marker-based motion capture systems using 95% functional limits of agreement in a linear mixed-effects modelling framework. Sci Rep. 2023;13(1). https://doi.org//10.1038/s41598-023-49360-2

21. Shen J, Zemiti N, Dillenseger JL, Poignet P. Fast And Simple Automatic 3D Ultrasound Probe Calibration Based On 3D Printed Phantom And An Untracked Marker. 2018 40th Annual International Conference of the IEEE Engineering in Medicine and Biology Society (EMBC). Published online July 2018:878-882. https://doi.org//10.1109/embc.2018.8512406

22. Ghorbani A, Ouyang D, Abid A, et al. Deep learning interpretation of echocardiograms. npj Digit Med. 2020;3(1). https://doi.org//10.1038/s41746-019-0216-8